Asian Journal of Chemistry; Vol. 36, No. 4 (2024), 802-810

ASIAN JOURNAL OF CHEMISTRY

https://doi.org/10.14233/ajchem.2024.31201

Improving Photocatalytic Performance through Incorporation of Various Cations in A-site of Double Perovskite Material $(Cs_{0.50}MA_{0.50})_2SnI_6$ for Degradation of Methylene Blue Dye Pollutant under Visible Light Irradiation

R. RAJA[1], J. JOHN SUNIL MANOAH[2], M. VIJAYAN[3] and R. GANESAN[1,*]

[1]Department of Physics, S.A. Engineering College (Autonomous), Chennai-600077, India
[2]Department of English, S.A. Engineering College (Autonomous), Chennai-600077, India
[3]Department of Physics, Vel Tech MultiTech Dr. Rangarajan Dr. Sakunthala Engineering College (Autonomous), Chennai-600062, India

*Corresponding author: E-mail: ganesanr@saec.ac.in; ganeshphy1986@gmail.com

Received: 10 January 2024; *Accepted*: 20 February 2024; *Published online*: 30 March 2024; AJC-21576

In this article, undoped double perovskite materials like caesium tin iodide (Cs_2SnI_6), methyl ammonium tin iodide [MA_2SnI_6: MA denotes $CH_3NH_3^+$] and mixed double perovskite material [$(Cs_{0.50}MA_{0.50})_2SnI_6$] were synthesized using a wet chemical methodology. The crystal structure confirmation, optical properties, thermal properties, surface morphology and presence of elemental composition of the prepared samples using XRD, UV, TGA and FESEM-EDAX analyses were thoroughly investigated. The synthesized materials were employed as photocatalysts to degrade methylene blue dye within 120 min under visible light. An increase in the optical properties of the synthesized double perovskite materials was confirmed by ultraviolet (UV) analysis, which showed that the introduction of various cations into the perovskite material at the A-site shifted the photoluminescence (PL) emission peak to the red. TGA results demonstrated that $(Cs_{0.50}MA_{0.50})_2SnI_6$ has greater thermal stability, which was confirmed by the presence of 43% of sample despite the temperature reaching almost 870 ºC. Doped double perovskite material $(Cs_{0.50}MA_{0.50})_2SnI_6$ exhibited increased photocatalytic activity, with methylene blue dye degradation efficiency attaining 89% after 120 min of visible light irradiation, which is greater than pure double perovskite materials. The photocatalytic degradation of methylene blue dye is mostly facilitated by hydroxyl radicals and holes, according to a radical trapping experiment that we conducted by employing different scavengers. The results of the current work showed that doped double perovskite materials [$(Cs_{0.50}MA_{0.50})_2SnI_6$] exhibit high thermal stability as well as higher photocatalytic activity than pure double perovskite materials. A possible photocatalytic reaction process is also diagrammatically using the band positions of double perovskite materials found using Mott-Schottky plots , which confirms that the synthesized double perovskite material has an N-type semiconductor nature.

Keywords: Double perovskite materials, Methylene blue dye, Wet chemical method, Photocatalyst, Optical property.

INTRODUCTION

Effluents from the textile, dyeing, printing and cosmetics industries have contaminated water, which has become one of the most polluted bodies of water due to the massive expansion of industries and technologies in recent years [1,2]. Methylene blue dye, for example, is commonly used as a dye in various industrial sectors such as textile, food and chemical industries and it can mix with and pollute domestic water [3,4]. Eliminating these contaminants is essential for preserving ecosystems, human health, and the environment due to the hazardous and non-biodegradable properties of these chemicals. As a result, it is critical to remove this toxic dye from contaminated water by converting it to inorganic, non-polluting compounds using photocatalyst materials mixed with wastewater. Organic dyes may trigger a variety of side effects, including but not limited to feeling dizzy, increased perspiration, nausea, vomiting, stomach discomfort, diarrhoea, an upset stomach or stomach cramps. Ingestions of methylene blue in high quantities might result in chest pain and confusion [5,6]. As a result, the development of highly efficient and environmentally friendly technologies for improving organic dye treatment processes is critical for cleaner production and long-term sustainability. Various technologies, including adsorption, biodegradation and advanced oxidation, have been proposed in this regard [7-10].

Photocatalysis technology is an advanced oxidation technology that uses radiation energy to perform photocatalytic degradation of dyes from water sources without producing more poisonous byproducts [11-13]. In photocatalytic treatment, semiconductors that are photoexcited by radiation with an energy level higher than their band gap are used [14,15]. Highly reactive oxygen species such as $OH^{\bullet}$ and $O_2^{\bullet}$ could be produced from photo-generated electrons and holes under these conditions. TiO_2, ZnS and ZnO are common semiconductor materials used in the dye degradation process [16]. Titanium oxide (TiO_2) has been used as one of the most attractive materials among these different semiconductor photocatalysts for many reasons, including high stability, resistance to different pH conditions, non-toxicity, strong redox reaction potentiality, low cost and market availability [2,11]. Unfortunately, because of its large band gap of more than 3.2 eV, conventional TiO_2 is active and can only be used under UV illumination, which accounts for only a small fraction of the sun's energy (5%) [12,13]. Visible light, on the other hand, accounts for nearly 45% of all available solar radiation. As a result, in order to use solar energy in photocatalytic processes because it is a renewable, green and low cost light source, photocatalysts that can activate in the visible region must be synthesized. As a result, by utilizing novel visible-light using active photocatalysts, sunlight would be used more efficiently and overall solar-based applications would be greatly improved [14-17]. Thus, designing new and highly efficient visible-light active photocatalysts for practical applications appears to be profitable. As a result, the new lead-free halide perovskite material has practical significance as a visible light photocatalyst for organic dye degradation. Double perovskite structures possess exceptional characteristics such high temperature stability, non-toxicity, high electrical conductivity, oxygen storage capability, considerable tunneling magneto resistance and magneto-dielectric effects, making them potential alternative materials for photocatalysts [18-20].

Recently, many researchers have utilized perovskite-based materials as photocatalysts to degrade organic dye solutions due to the well-established catalytic characteristics of perovskite structures. Zhang *et al.* [21] developed a simple wet chemical method for producing bare $MASnI_3$ and doped $MASnI_3/TiO_2$ photocatalysts and found that after 40 min of light irradiation, doped $MASnI_3/TiO_2$ had a photodegradation efficiency of rhodamine B (97%), which was higher than pure $MASnI_3$ and pure TiO_2. The increased photocatalytic activity is due to improved light-collecting ability and easy transfer of photo-generated carriers because of a decrease in the energy bandgap position between $MASnI_3$ and TiO_2. It has also been reported that lead-free $Cs_2AgSnCl_6$ double perovskite exhibits high photocatalytic activity by degrading 98.5% water-insoluble carcinogen Sudan Red III after 16 min of exposure to light and has good stability for 5-cycle operations [22]. A simple hydrothermal synthetic approach was used to develop doped rGO/$SrTiO_3$ for photocatalytic applications. Under UV-visible light irradiation, the degradation efficiency of these photocatalysts reached 91% for methylene blue dye and 81% for 2- nitrophenol, respectively [23]. Azar *et al.* [24] also investigated the photodegradation ability of $ZnTiO_3$ nanocomposite perovskite material and achieved more than 93% degradation of crystal violet and rhodamine B dyes as pollutant in 180 min under natural sunlight irradiation . The sol-gel citrate method was used to synthesize the novel double perovskite oxide Dy_2CoMnO_6 material and the results show that DCMO nanoparticles exhibit remarkable photocatalytic efficiency, degrading rhodamine-B by almost 98% in 4 h under visible irradiation [25]. Similarly, Bresolin *et al.* [26] prepared the novel methylammonium iodobismuthate perovskite material was successfully prepared using a low-temperature solvothermal method and the results showed that the increase in photocatalytic activity towards the values of removal was higher for rhodamine B than for the other dyes, with a removal of 98% after 3 h under visible light irradiation.

Previous research has not extensively explored the use of tin-based double perovskite materials as photocatalysts. In this regard, we synthesised doped and undoped tin-based double perovskite materials using a wet chemical method and they were used for photocatalyst applications as well as photocatalyst studies to compare the degradation efficiency of methylene blue dye under visible light radiation. The results show that doped double perovskite materials showed better photocatalytic activity than undoped double perovskite materials in the dye degradation process.

EXPERIMENTAL

Caesium iodide (CsI), tin iodide (SnI_2) and methyl ammonium iodide (MAI) were purchased with 99% purity from Sigma-Aldrich, USA and used without further purification. Caesium tin iodide (Cs_2SnI_6) was synthesised by wet chemical using CsI and SnI_2 as precursors in a 1:1 molar ratio and then dissolved in solvent (deionized water). To obtain a clear solution, 0.1 M HCl was added to SnI_2 solution. The prepared solution was stirred for 60 min to obtain perovskite material. These solutions were then exposed to air after being stirred. Since $CsSnI_3$ is typically unstable in air, it can be easily oxidized to Cs_2SnI_6 *via* a phase change. The resulting powder was tested in a hot air oven at 120 ºC for 24 h. Finally, pure white minute nanocrystals of Cs_2SnI_6 were obtained [27-29]. The other two perovskite nanocrystals [(MA_2SnI_6) and $(Cs_{0.50}MA_{0.50})_2SnI_6$] were prepared using the same method, by mixing stoichiometric amounts of their respective chloride salts.

Photocatalytic experiment: The degradation of methylene blue dye under visible light irradiation was used to investigate the photocatalytic activity of the prepared double perovskite materials. The photocatalytic experiment was carried out by exposing methylene blue dye solution (40 mL, 40 mg L^{-1}) to visible light irradiation in the presence of 40 mg Cs_2SnI_6, MA_2SnI_6 and incorporated caesium with methyl ammonium perovskite materials. The visible light source for dye degradation process was an Osram lamp with a wavelength range of 380 nm to 700 nm and a frequency range of 4×10^{14} to 8×10^{14} cycles per second, with a distance of 15 cm between the light source and the reaction solution. The solutions were thoroughly mixed in the dark for 30 min to achieve adsorption-desorption equilibrium between the photocatalyst particles and dye molecules. The photocatalytic reaction was then started by illuminating the dye solution with visible light for 120 min.

Every 30 min, 3 mL of the dye solution was collected and the concentration of the dye solution was measured using a UV-vis spectrometer with a maximum wavelength of 420 nm.

The radical trapping experiment was carried out using three different scavengers such as benzoquinone (BQ), disodium salt ethylenediaminetetraacetic acid (EDTA-2Na) and isopropanol (IPA) to learn about the predominant active participants involved in the dye degradation process and then samples were collected every 30 min up to 120 min and its UV-Visible spectrum absorption changes were analyzed. The spectrum helped to identify more dye degradation active species.

Characterization techniques: X-ray diffraction (XRD) pattern was obtained at room temperature using Bruker- AXS D8 Advance X-ray diffractometer with Cu*K*α radiation (λ = 1.54186 Å) to study the crystal structure of the prepared samples. The thermal stability of Cs_2SnI_6, MA_2SnI_6 and $(Cs_{0.50}MA_{0.50})_2SnI_6$ was investigated using Perkin-Elmer Diamond TGA instrument in a nitrogen atmosphere with the temperature range from 30 to 900 ºC. The optical properties and band gap values of synthesized perovskite materials were determined using a Varian Cary 6000i UV-vis-NIR spectrometer. Photoluminescence spectrum of synthesised double perovskite materials was employed using a home-built system combined with a 532 nm CW laser and a Si photodetector, respectively. The surface morphology and elemental presence in synthesised double perovskite materials were investigated using a FESEM and an EDAX spectrum (model CARL ZEISS SUPRA 55, Germany). The photocatalytic experiment for the synthesized double perovskite materials was carried out with visible light irradiation using 60 W Osram lamps.

RESULTS AND DISCUSSION

XRD studies: The crystallinity of the synthesized double perovskite materials was examined using XRD technique. An XRD measurement is shown in Fig. 1a for Cs_2SnI_6 perovskite material. The pure Cs_2SnI_6 exhibited diffraction peaks at 2θ values of 13.17º, 21.50º, 30.72º, 34.46º, 37.86º, 44.00º, 49.53º, 52.12º, 56.45º, 59.42º, 61.16º, 68.39º, corresponds to the (111), (220), (222), (420), (422), (440), (620), (622), (711), (642), (731), (822) lattice planes of cubic perovskite with lattice parameter $a = b = c = 11.63$ Å, respectively. As shown in Fig. 1a, all the obtained peaks are well matched with the JCPDS card file no. 730330 and earlier work [30-32]. Fig. 1b shows XRD spectrum of MA_2SnI_6 double perovskite material. For pure MA_2SnI_6, we observed strong diffraction peak at 2θ values 13.17º, 15.23º, 26.42º, 30.12º, 34.21º, 53.06º corresponds to the atomic planes of (111), (002), (222), (004), (044) and (444) face-centered cubic perovskite structure with its lattice constant was measured to be 12.016 Å, which was larger than that of Cs_2SnI_6 (11.63 Å) because the MA cation is larger than the Cs atom, respectively, which is well-matched with already reported literature [33,34]. The enhanced peak intensity of the (001) lattice plane is due to the high concentration of methyl ammonium cations [35]. These XRD investigations demonstrated that the synthesized double perovskite materials are methylammonium and caesium tin halide, respectively.

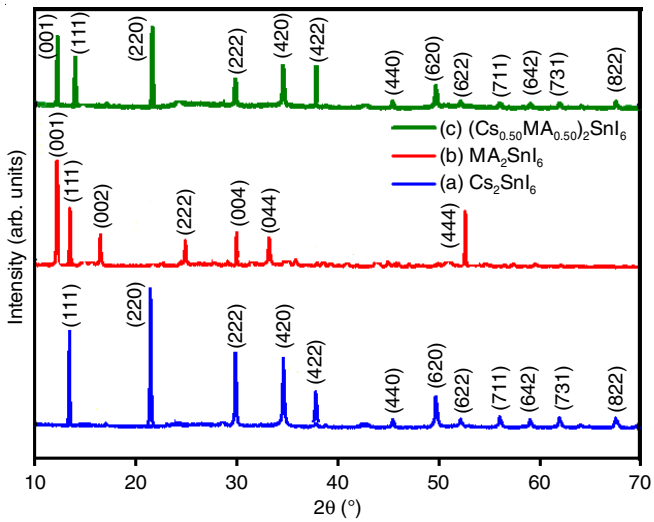

Fig. 1. XRD pattern of synthesized double perovskite materials (a) Cs_2SnI_6, (b) MA_2SnI_6 and (c) $(Cs_{0.50}MA_{0.50})_2SnI_6$

The XRD pattern of doped double perovskite material $(Cs_{0.50}MA_{0.50})_2SnI_6$ is shown in Fig. 1c. All the peaks are identical to the peaks found in Cs_2SnI_6, although the peak obtained at 2θ value 12.06º corresponding to lattice plane (001) is somewhat diminished when compared to the peak obtained in the same position in MA_2SnI_6. The peak has shrunk as the concentration of methylammonium in $(Cs_{0.50}MA_{0.50})_2SnI_6$ has decreased. When compared to the peaks obtained in pure Cs_2SnI_6 perovskite, the position of the peaks obtained in doped perovskite is slightly shifted towards a higher angle, which is due to an increase in lattice size, most likely because the ionic radius of MA^+ as the A-site cation was larger than that of Cs^+ [36,37].

UV studies: The ability of photocatalytic activity of produced double perovskite materials is dependent on light absorption. As a result, UV-Vis absorption of samples was conducted to determine the light absorption spectra of synthesized perovskite materials. Fig. 2a-c shows the absorbance spectra of Cs_2SnI_6, MA_2SnI_6 and $(Cs_{0.50}MA_{0.50})_2SnI_6$ measured in the wavelength range of 200-800 nm to determine the optical properties. For all the synthesized double perovskite materials a significant

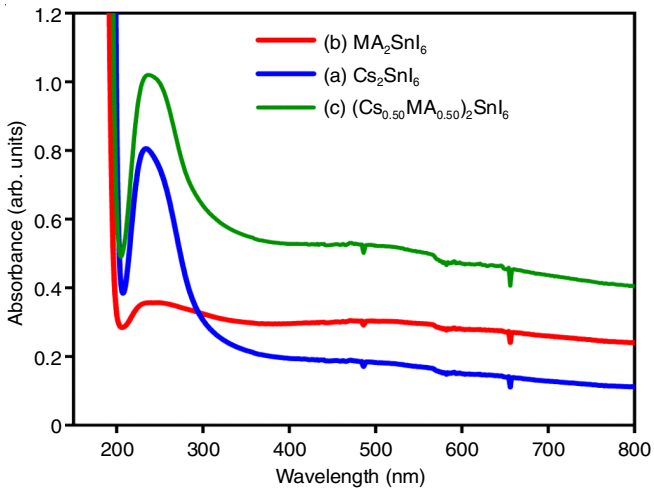

Fig. 2. UV-visible absorption spectra of synthesized double perovskite materials (a) Cs_2SnI_6, (b) MA_2SnI_6 and (c) $(Cs_{0.50}MA_{0.50})_2SnI_6$

amount of absorption occurs in the UV range of 200-300 nm wavelengths. Whereas, the broad absorption band appeared in visible region with wavelength range from 400-800 nm for all the synthesized double perovskite materials. But these obtained absorption peak is high for doped perovskite material $(Cs_{0.50}MA_{0.50})_2SnI_6$ while compared with other two perovskite materials. Hence, the optical properties were improved for caesium doped with methyl ammonium [$(Cs_{0.50}MA_{0.50})_2SnI_6$], because of its increase in light absorption peak [38,39].

The bandgap of all the synthesized perovskite materials were estimated using Tauc plot in which the variation of $(\alpha h\nu)^2$ and photon energy ($h\nu$) were plotted (Fig. 3a-c). From Tauc plot, the band gap values for MA_2SnI_6, Cs_2SnI_6 and $(Cs_{0.50}MA_{0.50})_2SnI_6$ were estimated to be 1.87, 1.70 and 1.65 eV, respectively, which is in a good agreement with previous reports [40-43]. The band gap was found to be 1.65 eV for $(Cs_{0.50}MA_{0.50})_2SnI_6$, which is smaller than that of other two pure double perovskite materials such as Cs_2SnI_6 (1.70 eV) and MA_2SnI_6 (1.87 eV). Therefore, doped perovskite material [$(Cs_{0.50}MA_{0.50})_2SnI_6$] could absorb maximum light because of lower bandgap value obtained. This result strongly indicates that photocatalytic activity was improved for doped perovskite materials compared with pure perovskite materials. Hence, the photocatalytic activity of the synthesized perovskite materials was performed towards the degradation of methylene blue dye under visible light irradiation.

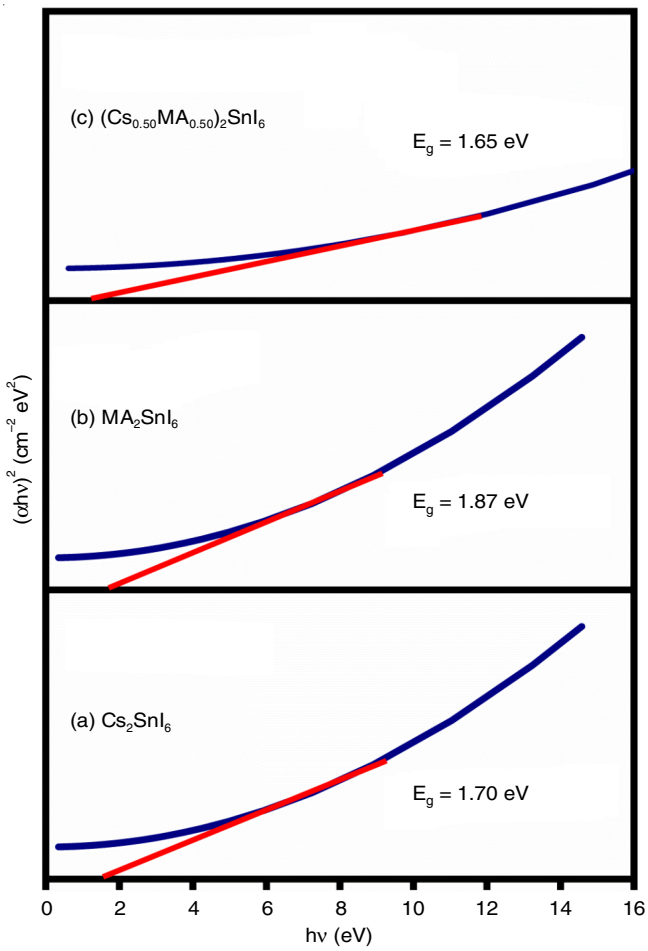

Fig. 3. Band gap values obtained from Tauc plot for synthesized double perovskite materials (a) Cs_2SnI_6, (b) MA_2SnI_6 and (c) $(Cs_{0.50}MA_{0.50})_2SnI_6$

Photoluminescence (PL) studies: Synthesized double perovskite materials MA_2SnI_6, Cs_2SnI_6 and $(Cs_{0.50}MA_{0.50})_2SnI_6$ are shown in Fig. 4 with their respective photoluminescence spectra, respectively. The incorporation of caesium with methyl ammonium cation in the A-site of double perovskite material caused the emission peak obtained for synthesized materials to shift towards longer wavelength, resulting in red shift, which indicates lower bandgap. The bandgap values obtained from the graph for the emission peak wavelength are in good agreement with band gap value calculated from the Tauc plot and previously reported work [32,34,44,45]. Based on the PL and absorption measurements, it is possible to conclude that the synthesized double perovskite materials have direct band gap values ranging from 1.54 to 1.87 eV, which is due to an equal proportion of caesium and methylammonium incorporation at the A-site of the double perovskite material.

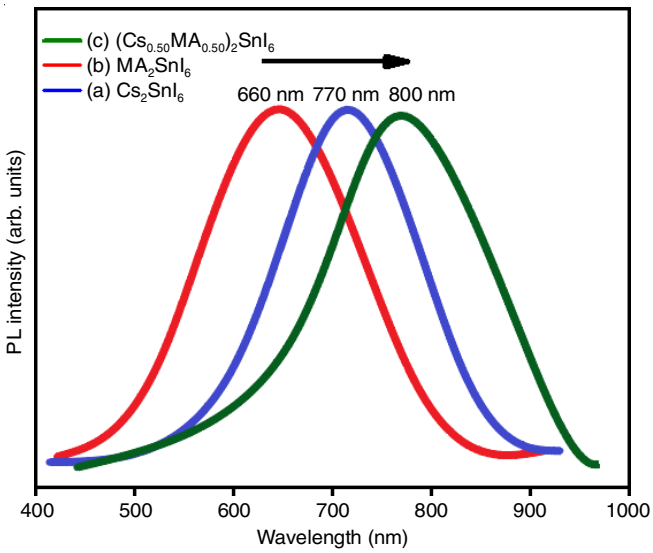

Fig. 4. PL spectrum for synthesized double perovskite materials (a) Cs_2SnI_6, (b) MA_2SnI_6 and (c) $(Cs_{0.50}MA_{0.50})_2SnI_6$

Thermogravimetric (TGA) studies: TGA studies under nitrogen flow from 30 to 900 ºC of Cs_2SnI_6, MA_2SnI_6 and $(Cs_{0.50}MA_{0.50})_2SnI_6$ are shown in Fig. 5a-c. According to Fig. 5a, the thermal decomposition of Cs_2SnI_6 begins about 300 ºC, where it decomposes into CsI and volatile SnI_4 [44]. This material loses weight continually until 24% of sample remains at 500 ºC and then there is no weight loss up to 900 ºC. As a result, this material Cs_2SnI_6 is stable up to 300 ºC. Fig. 5b indicates that MA_2SnI_6 is thermally stable up to 227 ºC and thereafter loses weight owing to decomposition of MA_2SnI_6 into MAI_2 and SnI_2 that may occur during the process [35,45]. From 227 to 400 ºC, the compound continues to decrease weight until around 80% is disappeared, which means that the residual chemical is mostly consist of SnI_4 [46-48].

Fig. 5c shows that a minor weight loss occurs about 250 ºC due to the presence of methylammonium cation in doped double perovskite $(Cs_{0.50}MA_{0.50})_2SnI_6$ material. Following that, the weight loss occurred gradually as temperature increased, with 43% of sample remaining available even when the temperature reached almost 870 ºC. As a result, the present research

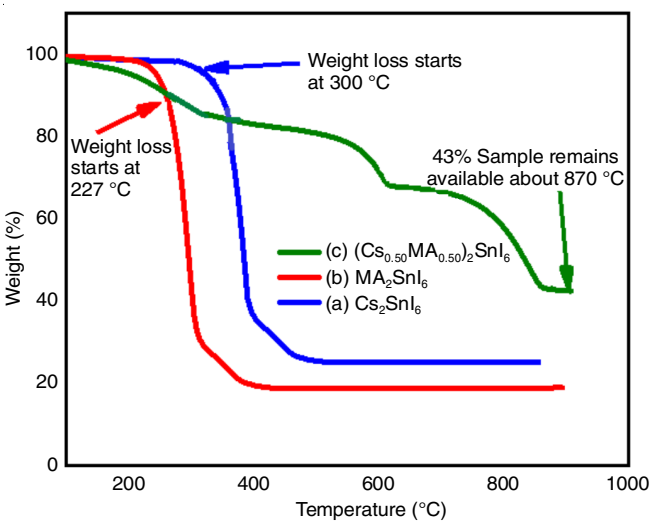

Fig. 5. TGA studies of synthesized double perovskite materials (a) Cs_2SnI_6, (b) MA_2SnI_6 and (c) $(Cs_{0.50}MA_{0.50})_2SnI_6$

demonstrates that doped perovskite material $(Cs_{0.50}MA_{0.50})_2SnI_6$ has higher thermal stability than undoped double perovskite materials.

FESEM/EDAX studies: The surface morphologies of synthesized double perovskite materials were analyzed by scanning electron microscopy (SEM) as shown in Fig. 6a-c. All of the double perovskite produced are nanosized and the catalyst particle size may be somewhat reduced by the addition of caesium with methylammonium cation [29]. Smaller particle sizes allow for easier charge transport, resulting in more electron-hole pairs, which improves the photocatalytic activity of doped double perovskite material $(Cs_{0.50}MA_{0.50})_2SnI_6$ [49-51]. Fig. 7a-c depicts the presence of elements in Cs_2SnI_6, MA_2SnI_6 and $(Cs_{0.50}MA_{0.50})_2SnI_6$. The presence of components Cs, Sn and I reveals that the synthesized double perovskite is Cs_2SnI_6 [45], whereas the existence of N, C, Sn and I components in Fig. 7b demonstrates that the synthesized powder is MA_2SnI_6 [47]. Similarly, the presence of Cs, Sn, I, N and C elements, as shown in Fig. 7c, indicates that the synthesized material is an incorporation of both caesium and methyl ammonium tin halide at the A-site of double perovskite material $[(Cs_{0.50}MA_{0.50})_2SnI_6]$.

Photocatalyst studies: The synthesized double perovskite materials were tested for their photocatalytic activity using methylene blue (MB) dye, a common dye found in textile industry wastewater and often used as a standard pollutant for photocatalytic experiments, under visible light irradiation. The activity was evaluated against 3 ppm MB with 40 mg of catalyst added. At first, a UV-visible spectrophotometer was used to measure the absorbance at regular intervals after mixing the dye-catalyst and then agitated the solution in dark. The reduction of the MB absorption peak prior to visible light irradiation (dark reaction) suggests MB adsorption on the catalysts. Fig. 8a-c depicts photocatalytic degradation of Cs_2SnI_6, MA_2SnI_6 and $(Cs_{0.50}MA_{0.50})_2SnI_6$ defect perovskite materials produced. The spectra show a minor fluctuation with generated samples observed at 30 min intervals. The dye degraded under steady UV light irradiation and the colour degradation was constantly recorded until the colour disappears completely. The decolourization suggests that the dye's absorption band has been dimin-

Fig. 6. FESEM images for synthesized double perovskite materials (a) Cs_2SnI_6, (b) MA_2SnI_6 and (c) $(Cs_{0.50}MA_{0.50})_2SnI_6$

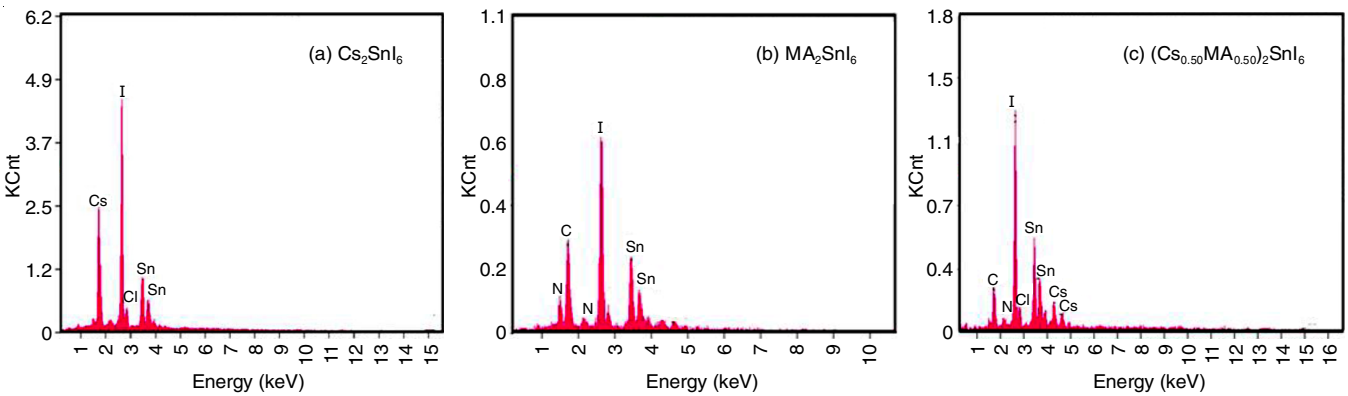

Fig. 7. EDAX spectrum for synthesized double perovskite materials (a) Cs_2SnI_6, (b) MA_2SnI_6 and (c) $(Cs_{0.50}MA_{0.50})_2SnI_6$

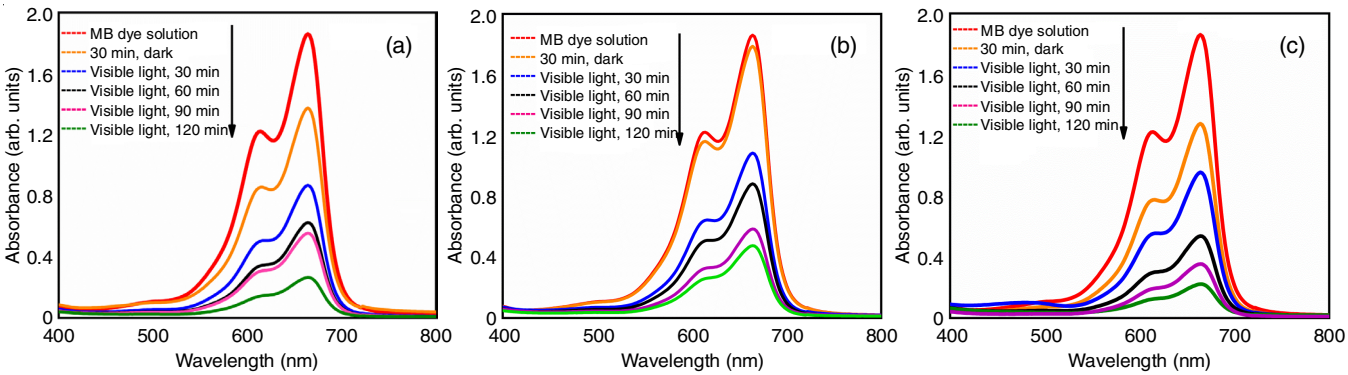

Fig. 8. Absorption spectra for methylene blue dye degradation by synthesized double perovskite materials (a) Cs_2SnI_6, (b) MA_2SnI_6 and (c) $(Cs_{0.50}MA_{0.50})_2SnI_6$

ished by light exposure, with the absorption band nearly disappeared after 120 min of light exposure for $(Cs_{0.50}MA_{0.50})_2SnI_6$ compared to perovskite materials without any additional substances. The results showed that the degradation of MB dye for $(Cs_{0.50}MA_{0.50})_2SnI_6$ was higher than for the other two perovskites, MA_2SnI_6 and Cs_2SnI_6.

The methylene blue degradation (photocatalytic efficiency) was achieved after 120 min of light irradiation at 74%, 85% and 89% for MA_2SnI_6, Cs_2SnI_6 and $(Cs_{0.50}MA_{0.50})_2SnI_6$, respectively. The photocatalytic effectiveness of $(Cs_{0.50}MA_{0.50})_2SnI_6$ increases owing to significant light absorption, considerable separation of electron-hole pairs and nanoparticle size.

Kinetic studies: The absorbance spectra gradually decrease as illumination duration increases. According to Lambert-Beer's rule, the reduction in dye concentration in the solution indicates dye degradation [52,53]. The photocatalytic activity of the defect perovskites MA_2SnI_6, Cs_2SnI_6 and $(Cs_{0.50}MA_{0.50})_2SnI_6$ is shown in Fig. 9a. According to this graph, the ratio of C_t/C_o decreases with increasing light irradiation period for all synthesized samples. Despite this, the C_t/C_o value for the doped double perovskite $(Cs_{0.50}MA_{0.50})_2SnI_6$ is lower at all times when compared to other perovskite materials. As a result, it demonstrates that mixed cation photocatalytic activity may be enhanced over undoped perovskite materials.

Furthermore, the investigation of photocatalytic reaction kinetics, as shown in Fig. 9b, reveals that the photocatalytic activity of the generated synthetic defect perovskite materials obeys first-order reaction kinetics as follows [54]:

$$-\log\frac{C_t}{C_o} = Kt$$

where C_t and C_o represent the concentrations of MB dye after and before the photocatalytic process, t represents the irradiation time and k represents the rate constant.

Photocatalytic degradation of methylene blue dye: Fig. 10a-c show that the usage of different scavengers like *p*-benzoquinone (BQ), ethylenediaminetetraacetic acid (EDTA-2Na) and isopropanol (IPA) reduces photodegradation efficiency from 74 to 68%, 46 and 26%, 85 to 70%, 52% and 30% and 89 to 72%, 55% and 32% for MA_2SnI_6, Cs_2SnI_6 and $(Cs_{0.50}MA_{0.50})_2SnI_6$, respectively. As demonstrated in Fig. 11a-c, the photodegradation of MB dye was greatly decreased when IPA and EDTA-2Na were added, but there was only a little reduction when BQ was introduced [55,56]. After 180 min of photocatalytic degradation with visible light, the MB degradation % is as follows: IPA > EDTA > BQ. This pattern implies that the primary oxidizing agent involved in the breakdown of MB is the OH. As a result, the formation of ROS occurs in the following order:

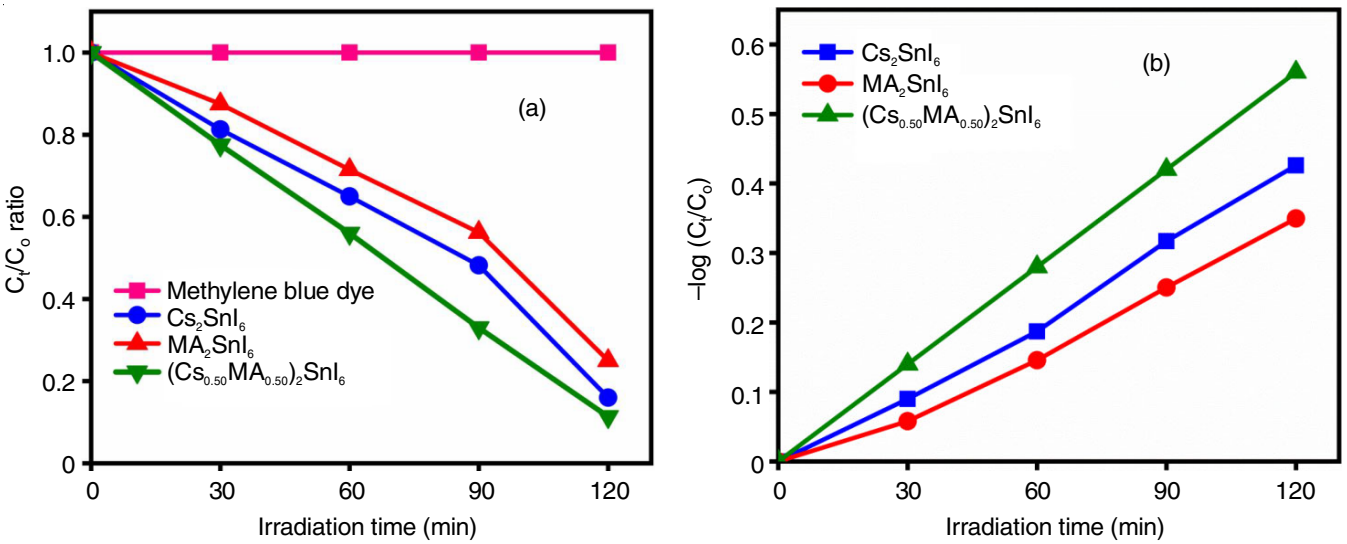

Fig. 9. (a) Degradation rate and (b) Kinetic fit of methylene blue dye under visible light irradiatio

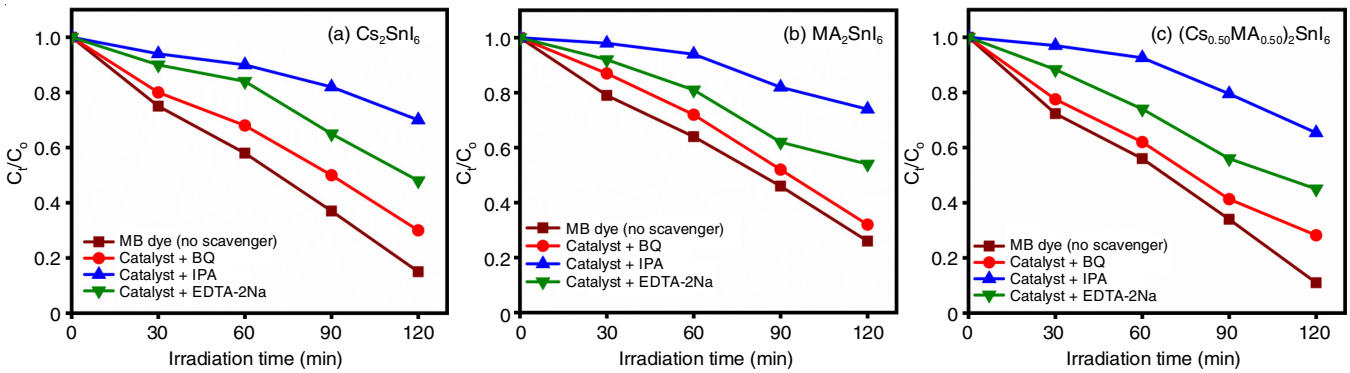

Fig. 10. Degradation rate of methylene blue dye in the presence of different scavengers with perovskite materials (a) Cs_2SnI_6, (b) MA_2SnI_6 and (c) $(Cs_{0.50}MA_{0.50})_2SnI_6$

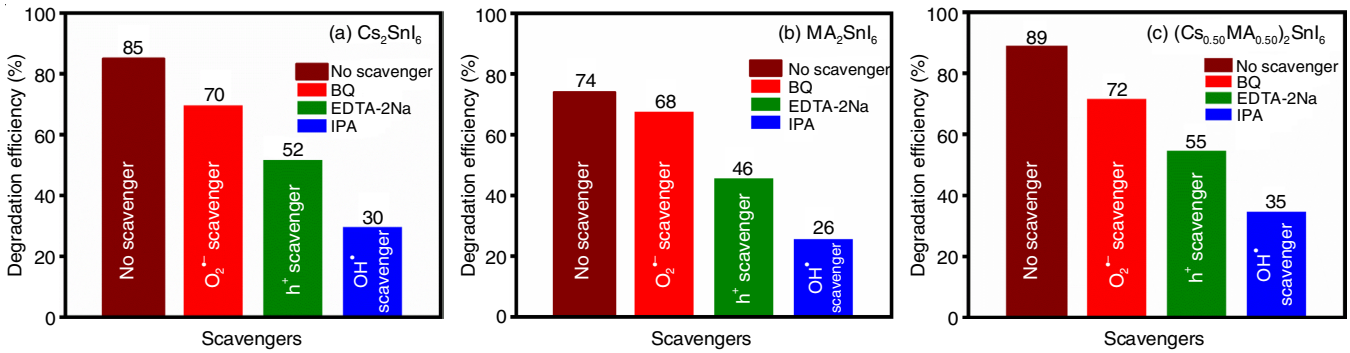

Fig. 11. Effect of different scavengers on methylene blue dye degradation for (a) Cs_2SnI_6, (b) MA_2SnI_6 and (c) $(Cs_{0.50}MA_{0.50})_2SnI_6$

$OH^\bullet > h^+ > O_2^{\bullet-}$. Finally, the trapping experiment revealed that the oxidation processes of hydroxyl radical and holes dominated the degradation of MB dye.

Mott-Schottky plot and proposed mechanism for the photocatalytic activity enhancement: To understand the photocatalytic mechanism of synthesized perovskite materials, the flat band potential (E_{fb}) of synthesized MA_2SnI_6, Cs_2SnI_6 and $(Cs_{0.50}MA_{0.50})_2SnI_6$ must be determined using a Mott-Schottky plot. The positive slope fitting line of the M-S plot in Fig. 12a-c indicates that the synthesized double perovskite materials exhibit N-type semiconductor nature [57,58]. The flat band potentials (E_{fb}) were calculated by intercepting the plot ($1/C^2 = 0$) on the *x*-axis, as shown in Fig. 12.

Using the flat band potential and optical band gap energy values, the valence band (VB) and conduction band (CB) positions were calculated. The CB bottom band positions for MA_2SnI_6, Cs_2SnI_6 and $(Cs_{0.50}MA_{0.50})_2SnI_6$ perovskite materials were obtained to be 0.45 V, 0.41 V and 0.36 V, respectively. Similarly, the VB edge potentials were found from the equation $E_{VB} = E_{CB} + E_g$ and these values were 2.32 V, 2.11 V and 2.01 V for MA_2SnI_6, Cs_2SnI_6 and $(Cs_{0.50}MA_{0.50})_2SnI_6$ materials, respectively [59].

Electrons are excited from the valance band and transferred to the conduction band (CB) upon exposure of the photocatalysts to light. This process resulted in the formation of holes in the valance band on both catalysts. Since for $(Cs_{0.50}MA_{0.50})_2SnI_6$, the CB edge band potential [0.36 V *vs.* NHE] is more positive than the typical redox potential ($O_2/O_2^{\bullet-}$) [- 0.33 eV *vs.* NHE], electrons at the CB could not change O_2 to $O_2^{\bullet-}$. As a result, as

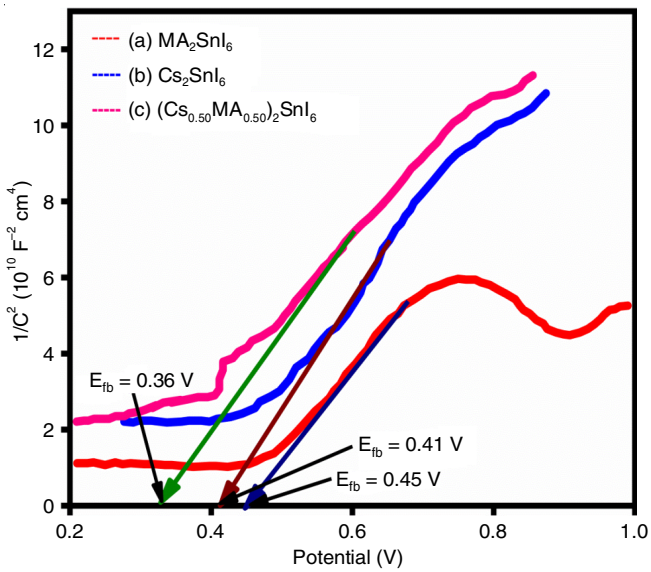

Fig. 12. Mott-Schottky plot of synthesized double perovskite materials (a) Cs_2SnI_6, (b) MA_2SnI_6 and (c) $(Cs_{0.50}MA_{0.50})_2SnI_6$

demonstrated by the elemental trapping experiment, the superoxide radicals are not active participants in the MB dye degradation process. The CB edge potential of $(Cs_{0.50}MA_{0.50})_2SnI_6$ is, however, more negative than the conventional redox potential (O_2/H_2O_2) (0.685 V *vs.* NHE), suggesting that oxygen adsorbed on the catalyst's surface can react with two electrons to generate H_2O_2. Following that H_2O_2 interacts with one electron to generate $^\bullet OH$, which has a strong oxidizing capacity and is involved in

photocatalytic activity [6]. Furthermore, the $(Cs_{0.50}MA_{0.50})_2SnI_6$ VB edge potential [2.01 V *vs.* NHE] is more positive than the standard redox potential of $^{\bullet}OH/OH^-$ [1.99 V *vs.* NHE], implying that the accumulating holes on the VB of $(Cs_{0.50}MA_{0.50})_2SnI_6$ may readily oxidize OH_{ads} to create $^{\bullet}OH$. These hydroxyl radicals ($^{\bullet}OH$) react with the MB dye to form a mineralized product, which is the primary active species in the degradation process and resulting in the exceptional photocatalytic activity [60]. According to the elemental radical trapping experiment, some of the holes may be directly involved in the oxidation of organic compounds. Based on the above discussion, the mechanism of MB dye degradation in the presence of perovskite materials when exposed to visible light can be explained as follows, which is also depicted diagrammatically in Fig. 13.

$$(Cs_{0.50}MA_{0.50})_2SnI_6 + h\nu \longrightarrow h^+_{VB} + e^-_{CB}$$

$$O_2 + 2e^- + 2H^+ \longrightarrow H_2O_2$$

$$H_2O_2 + e^- \longrightarrow {}^{\bullet}OH + OH$$

$$OH^-_{ads} + h^+ \longrightarrow {}^{\bullet}OH$$

$$OH^- + h^+ \longrightarrow {}^{\bullet}OH$$

$$\text{MB Dyes} + {}^{\bullet}OH, h^+ \longrightarrow CO_2 + H_2O$$

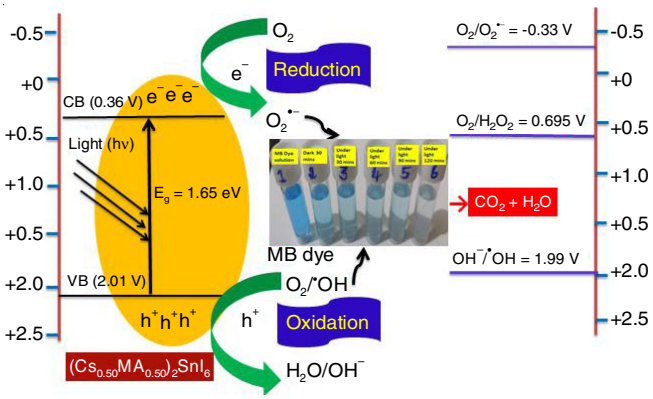

Fig. 13. Working diagram of photocatalyst process

Conclusion

In this study, undoped and doped double perovskite materials such as Cs_2SnI_6, MA_2SnI_6 and $(Cs_{0.50}MA_{0.50})_2SnI_6$ were synthesized successfully using wet chemical method for photocatalyst applications. The crystalline nature, optical properties, thermal stability, surface morphology and presence of elements in the synthesized perovskite materials were studied using XRD, UV, PL, TGA and FESEM-EDAX, respectively. The XRD analysis confirmed that the synthesized perovskite materials are well crystalline in nature. The optical investigations revealed that addition of caesium and methyl ammonium cations to the A-site of double perovskite material $(Cs_{0.50}MA_{0.50})_2SnI_6$ improves light absorption due to tunable bandgap values ranging from 1.65 to 1.87 eV, which is confirmed by photoluminescence (PL) spectra. The effect of various cation incorporation, which leads to considerably increased thermal stability for doped perovskite mixed halide material and it was confirmed based on the 43% of sample still available without loss even when temperature reached around 870 ºC. The photocatalytic results showed that doped perovskite material $(Cs_{0.50}MA_{0.50})_2SnI_6$ had exceptional photocatalytic activity for methylene blue dye degradation as compared to undoped perovskite materials, with a degradation efficiency of 89% after 120 min of visible light irradiation. The increased photocatalytic activity might be due to the production of additional electron-hole pairs as a result of widening the light absorption range *via* band gap tuning, which results in a red shift of the PL emission peak. In this study, the band position of synthesized perovskite materials has also been used to explain a proposed photocatalytic reaction mechanism. It was found that the hydroxyl and holes radicals were the primary active species in the methylene blue dye degradation process after conducting radical trapping experiments with various scavengers. These results suggest that a doped double perovskite material is a stable and efficient photocatalyst for the degradation of methylene blue dye when exposed to visible light and it might be a promising candidate for photocatalytic applications.

CONFLICT OF INTEREST

The authors declare that there is no conflict of interests regarding the publication of this article.

REFERENCES

1. B. Revathi, L. Balakrishnan, S. Pichaimuthu, A. Nirmala Grace and N. Krishna Chandar, *J. Mater. Sci. Mater. Electron.*, **31**, 22487 (2020); https://doi.org/10.1007/s10854-020-04750-4
2. P. Shirazi, M. Rahbar, M. Behpour and M. Ashrafi, *New J. Chem.*, **44**, 231 (2020); https://doi.org/10.1039/C9NJ04932K
3. S. Chandrasekhar and P.N. Pramada, *Adsorption*, **12**, 27 (2006); https://doi.org/10.1007/s10450-006-0136-1
4. S. Topcu Sendogdular, *J. Iran. Chem. Soc.*, **20**, 427 (2023); https://doi.org/10.1007/s13738-022-02677-7
5. A. Fernandez-Perez and G. Marban, *ACS Omega*, **5**, 29801 (2020); https://doi.org/10.1021/acsomega.0c03830
6. Z. Chen, X. Jiang, C. Zhu and C. Shi, *Appl. Catal. B*, **199**, 241 (2016); https://doi.org/10.1016/j.apcatb.2016.06.036
7. J. Sun, Z. Yang, L. Li, L. Zhang and G. Zou, *Environ. Sci. Pollut. Res. Int.*, **28**, 50813 (2021); https://doi.org/10.1007/s11356-021-14188-8
8. M. Manna and S. Sen, *Environ. Sci. Pollut. Res.*, **30**, 25477 (2023); https://doi.org/10.1007/s11356-022-19435-0
9. M. Ismael and M. Wark, *Catalysts*, **9**, 342 (2019); https://doi.org/10.3390/catal9040342
10. R. Abirami, T.S. Senthil and C.R. Kalaiselvi, *Solid State Commun.*, **327**, 114232 (2021); https://doi.org/10.1016/j.ssc.2021.114232
11. H.J. Jang, S.J. Park, J.H. Yang, S.M. Hong, C.K. Rhee, D. Kim and Y. Sohn, *Mater. Sci. Semicond. Process.*, **132**, 105919 (2021); https://doi.org/10.1016/j.mssp.2021.105919
12. G. Venkatesh, S. Prabhu, M. Geerthana, P. Baskaran, R. Ramesh and K.M. Prabu, *Optik*, **212**, 164716 (2020); https://doi.org/10.1016/j.ijleo.2020.164716
13. S. Li, L. Jing, W. Fu, L. Yang, B. Xin and H. Fu, *Mater. Res. Bull.*, **42**, 203 (2007); https://doi.org/10.1016/j.materresbull.2006.06.010
14. S. Das, T. Paul, S. Maiti and K.K. Chattopadhyay, *Mater. Lett.*, **267**, 127501 (2020); https://doi.org/10.1016/j.matlet.2020.127501
15. Z. Liu, H. Yang, J. Wang, Y. Yuan, K. Hills-Kimball, T. Cai, P. Wang, A. Tang and O. Chen, *Nano Lett.*, **21**, 1620 (2021); https://doi.org/10.1021/acs.nanolett.0c04148

16. R. Daghrir, P. Drogui and D. Robert, *Ind. Eng. Chem. Res.*, **52**, 3581 (2013); https://doi.org/10.1021/ie303468t
17. M. Abdi, V. Mahdikhah and S. Sheibani, *Opt. Mater.*, **102**, 109803 (2020); https://doi.org/10.1016/j.optmat.2020.109803
18. M. Irshad, Q. Ain, M. Zaman, M.Z. Aslam, N. Kousar, M. Asim, M. Rafique, K. Siraj, A.N. Tabish, M. Usman, M.H. Farooq, M.A. Assiri and M. Imran, *RSC Adv.*, **12**, 7009 (2022); https://doi.org/10.1039/D1RA08185C
19. G.W.K. Moore, S.E.L. Howell, M. Brady, X. Xu and K. McNeil, *Nat. Commun.*, **12**, 1 (2021); https://doi.org/10.1038/s41467-020-20314-w
20. B.M. Bresolin, C. Gunnemann, D.W. Bahnemann and M. Sillanpaa, *Nanomaterials*, **10**, 763 (2020); https://doi.org/10.3390/nano10040763
21. W. Zhang, Q. Zhao, X. Wang, X. Yan, J. Xu and Z. Zeng, *Catal. Sci. Technol.*, **7**, 2753 (2017); https://doi.org/10.1039/C7CY00389G
22. K. Li, S. Li, W. Zhang, Z. Shi, D. Wu, X. Chen, P. Lin, Y. Tian and X. Li, *J. Colloid Interface Sci.*, **596**, 376 (2021); https://doi.org/10.1016/j.jcis.2021.03.144
23. G. Venkatesh, S. Vignesh, M. Srinivasan, G. Palanisamy, N. Elavarasan, K. Bhuvaneswari, P. Ramasamy, M. Alam, M. Ubaidullah and M.K. Raza, *Colloids Surf. A Physicochem. Eng. Asp.*, **629**, 127523 (2021); https://doi.org/10.1016/j.colsurfa.2021.127523
24. T. Tavakoli-Azar, A.R. Mahjoub, M.S. Sadjadi, N. Farhadyar and M.H. Sadr, *Inorg. Chem. Commun.*, **119**, 108091 (2020); https://doi.org/10.1016/j.inoche.2020.108091
25. S. Chanda, R. Maity, S. Saha, A. Dutta and T.P. Sinha, *J. Sol-Gel Sci. Technol.*, **99**, 600 (2021); https://doi.org/10.1007/s10971-021-05605-y
26. B.M. Bresolin, S.B. Hammouda and M. Sillanpaa, *J. Photochem. Photobiol. Chem.*, **376**, 116 (2019); https://doi.org/10.1016/j.jphotochem.2019.03.009
27. P. Rawat, S.K. Saroj, M. Gupta, G. Vijaya Prakash and R. Nagarajan, *J. Fluor. Chem.*, **200**, 1 (2017); https://doi.org/10.1016/j.jfluchem.2017.05.008
28. A.S. Thind, S. Kavadiya, M. Kouhnavard, R. Wheelus, S.B. Cho, L.Y. Lin, C. Kacica, H.K. Mulmudi, K.A. Unocic, A.Y. Borisevich, G. Pilania, P. Biswas and R. Mishra, *Chem. Mater.*, **31**, 4769 (2019); https://doi.org/10.1021/acs.chemmater.9b01025
29. A.A. Kumar, J. Singh, D.S. Rajput, A. Placke, A. Kumar and J. Kumar, *Mater. Sci. Semicond. Process.*, **83**, 83 (2018); https://doi.org/10.1016/j.mssp.2018.04.023
30. X. Qiu, Y. Jiang, H. Zhang, Z. Qiu, S. Yuan, P. Wang and B. Cao, *Phys. Status Solidi Rapid Res. Lett.*, **10**, 587 (2016); https://doi.org/10.1002/pssr.201600166
31. X. Qiu, B. Cao, S. Yuan, X. Chen, Z. Qiu, Y. Jiang, Q. Ye, H. Wang, H. Zeng, J. Liu and M.G. Kanatzidis, *Sol. Energy Mater. Sol. Cells*, **159**, 227 (2017); https://doi.org/10.1016/j.solmat.2016.09.022
32. F. Guo, Z. Lu, D. Mohanty, T. Wang, I.B. Bhat, S. Zhang, S. Shi, M.A. Washington, G.C. Wang and T.M. Lu, *Mater. Res. Lett.*, **5**, 540 (2017); https://doi.org/10.1080/21663831.2017.1346525
33. T. Kinoshita, R. Kakeno and H. Segawa, *Chem. Lett.*, **48**, 637 (2019); https://doi.org/10.1246/cl.190165
34. F. Funabiki, Y. Toda and H. Hosono, *J. Phys. Chem. C*, **122**, 10749 (2018); https://doi.org/10.1021/acs.jpcc.8b01820
35. L. Dimesso, C. Das, T. Mayer and W. Jaegermann, *J. Mater. Sci.*, **53**, 356 (2018); https://doi.org/10.1007/s10853-017-1545-0
36. G. Murugadoss, R. Thangamuthu, S. Vijayaraghavan, H. Kanda and G. Ito, *Electrochim. Acta*, **257**, 267 (2017); https://doi.org/10.1016/j.electacta.2017.10.092
37. H. Choi, J. Jeong, H.B. Kim, S. Kim, B. Walker, G.H. Kim and J.Y. Kim, *Nano Energy*, **7**, 80 (2014); https://doi.org/10.1016/j.nanoen.2014.04.017
38. B. Lee, A. Krenselewski, S.I. Baik, D.N. Seidman and R.P. Chang, *Sustain. Energy Fuels*, **1**, 710 (2017); https://doi.org/10.1039/C7SE00100B
39. M.M. Tavakoli, L. Gu, Y. Gao, C. Reckmeier, J. He, A.L. Rogach, Y. Yao and Z. Fan, *Sci. Rep.*, **5**, 14083 (2015); https://doi.org/10.1038/srep14083
40. B. Lee, C.C. Stoumpos, N. Zhou, F. Hao, C. Malliakas, C.Y. Yeh, T.J. Marks, M.G. Kanatzidis and R.P. Chang, *J. Am. Chem. Soc.*, **136**, 15379 (2014); https://doi.org/10.1021/ja508464w
41. Z. Xiao, H. Lei, X. Zhang, Y. Zhou, H. Hosono and T. Kamiya, *Bull. Chem. Soc. Jpn.*, **88**, 1250 (2015); https://doi.org/10.1246/bcsj.20150110
42. P. Xu and F. Liu, *J. Appl. Phys.*, **129**, 125701 (2021); https://doi.org/10.1063/5.0045391
43. A.E. Maughan, A.M. Ganose, A.M. Candia, J.T. Granger, D.O. Scanlon and J.R. Neilson, *Chem. Mater.*, **30**, 472 (2018); https://doi.org/10.1021/acs.chemmater.7b04516
44. B. Saparov, J.P. Sun, W. Meng, Z. Xiao, H.S. Duan, O. Gunawan, D. Shin, I.G. Hill, Y. Yan and D.B. Mitzi, *Chem. Mater.*, **28**, 2315 (2016); https://doi.org/10.1021/acs.chemmater.6b00433
45. F. Hao, C.C. Stoumpos, D.H. Cao, R.P. Chang and M.G. Kanatzidis, *Nat. Photonics*, **8**, 489 (2014); https://doi.org/10.1038/nphoton.2014.82
46. Y. Dang, Y. Liu, Y. Sun, D. Yuan, X. Liu, W. Lu, G. Liu, H. Xia and X. Tao, *CrystEngComm*, **17**, 665 (2015); https://doi.org/10.1039/C4CE02106A
47. R. Ganesan, S.P. Vinodhini, V. Balasubramani, G. Parthipan, T.M. Sridhar, R. Arulmozhi and R. Muralidharan, *New J. Chem.*, **43**, 15258 (2019); https://doi.org/10.1039/C9NJ03902C
48. J.C.-R. Ke, D.J. Lewis, A.S. Walton, B.F. Spencer, P. O'Brien, A.G. Thomas and W.R. Flavell, *J. Mater. Chem. A Mater. Energy Sustain.*, **6**, 11205 (2018); https://doi.org/10.1039/C8TA03133A
49. J. Liu, J. Lin, Q. Xue, Q. Ye, X. He, L. Ouyang, D. Zhuang, C. Liao, H.L. Yip, J. Mei and W.M. Lau, *J. Power Sources*, **301**, 242 (2016); https://doi.org/10.1016/j.jpowsour.2015.10.023
50. S.M. Jain, D. Phuyal, M.L. Davies, M. Li, B. Philippe, C. De Castro, Z. Qiu, J. Kim, T. Watson, W.C. Tsoi, O. Karis, H. Rensmo, G. Boschloo, T. Edvinsson and J.R. Durrant, *Nano Energy*, **49**, 614 (2018); https://doi.org/10.1016/j.nanoen.2018.05.003
51. M.A. Najeeb, Z. Ahmad, R.A. Shakoor, A. Alashraf, J. Bhadra, N.J. Al-Thani, S.A. Al-Muhtaseb and A.M.A. Mohamed, *Opt. Mater.*, **73**, 50 (2017); https://doi.org/10.1016/j.optmat.2017.07.043
52. R. Ganesan, R. Muralidharan, S.P. Vinodhini, V. Balasubramani, T.M. Sridhar, G. Parthipan, R. Arulmozhi and H. Leelavathi, *J. Mater. Sci. Mater. Electron.*, **32**, 25409 (2021); https://doi.org/10.1007/s10854-021-07001-2
53. B.M. Bresolin, P. Sgarbossa, D.W. Bahnemann and M. Sillanpaa, *Sep. Purif. Technol.*, **251**, 117320 (2020); https://doi.org/10.1016/j.seppur.2020.117320
54. S.M. Yakout, *J. Solid State Chem.*, **290**, 121517 (2020); https://doi.org/10.1016/j.jssc.2020.121517
55. X. Xu, M. Lv, X. Sun and G. Liu, *J. Mater. Sci.*, **51**, 6464 (2016); https://doi.org/10.1007/s10853-016-9945-0
56. S. Halder, M.S. Sheikh, R. Maity, B. Ghosh and T.P. Sinha, *Ceram. Int.*, **45**, 15496 (2019); https://doi.org/10.1016/j.ceramint.2019.05.053
57. R. Maity, M. Sheikh, A. Dutta and T.P. Sinha, *J. Electron. Mater.*, **48**, 4856 (2019); https://doi.org/10.1007/s11664-019-07285-5
58. S. Demirel, R. Topkaya and K. Cicek, *J. Mater. Sci. Mater. Electron.*, **34**, 1 (2023); https://doi.org/10.1007/s10854-022-09392-2
59. W. Meng, R. Hu, J. Yang, Y. Du, J. Li and H. Wang, *Chin. J. Catal.*, **37**, 1283 (2016); https://doi.org/10.1016/S1872-2067(16)62449-X
60. S. Gulati, K. Goyal, A. Arora, S. Kumar, M. Trivedi and S. Jain, *Environ. Sci. Water Res. Technol.*, **8**, 1590 (2022); https://doi.org/10.1039/D2EW00027J